

MotionSC: Data Set and Network for Real-Time Semantic Mapping in Dynamic Environments

Joey Wilson, Jingyu Song, Yuewei Fu, Arthur Zhang
Andrew Capodiecici, Paramsothy Jayakumar, Kira Barton, and Maani Ghaffari

Abstract—This work addresses a gap in semantic scene completion (SSC) data by creating a novel outdoor data set with accurate and complete dynamic scenes. Our data set is formed from randomly sampled views of the world at each time step, which supervises generalizability to complete scenes without occlusions or traces. We create SSC baselines from state-of-the-art open source networks and construct a benchmark real-time dense local semantic mapping algorithm, MotionSC, by leveraging recent 3D deep learning architectures to enhance SSC with temporal information. Our network shows that the proposed data set can quantify and supervise accurate scene completion in the presence of dynamic objects, which can lead to the development of improved dynamic mapping algorithms. All software is available at <https://github.com/UMich-CURLY/3DMapping>.

I. INTRODUCTION

3D scene understanding is a keystone for mobile robotics. Scene understanding enables a robot to reason the environment and improve decision-making, internal navigation, path planning, and control execution. While 2D scene understanding is useful for robots, a 3D understanding ultimately provides an opportunity for significantly more information, e.g., navigating under obstacles or understanding their size. Therefore, 3D scene understanding is necessary for autonomous vehicles [1], as the 2D information cannot support certain robotic applications due to the lack of depth information.

Scene understanding is generally broken into sub-tasks due to its broad scope, including object detection, scene categorization, semantic segmentation, depth estimation, tracking, and prediction [2]. These tasks are easier to conquer on their own, and have seen significant progress in recent years due to the development of 3D deep learning networks and rapid improvement of 3D sensors. The main challenges still facing 3D deep learning include memory and computation restrictions and working with sparse and unstructured data such as point clouds [3]. Additionally, these sub-tasks are more straightforward to produce ground truth labels for than higher-level scene understanding tasks such as semantic scene completion, where a ground truth map of the world is nearly impossible to attain in outdoor, dynamic scenes [1].

DISTRIBUTION A. Approved for public release; distribution unlimited. OPSEC #6152

J. Wilson, J. Song, Y. Fu, A. Zhang, K. Barton, and M. Ghaffari are with the University of Michigan, Ann Arbor, MI 48109, USA. {wilsoniv, jingyuso, ywfu, arthurzh, bartonkl, maanigj}@umich.edu.

A. Capodiecici is with Neya Systems Division, Applied Research Associates, Warrendale, PA 15086, USA. acapodiecici@neyarobotics.com.

P. Jayakumar is with the US Army DEVCOM Ground Vehicle Systems Center, Warren, MI 48397, USA. paramsothy.jayakumar.civ@army.mil.

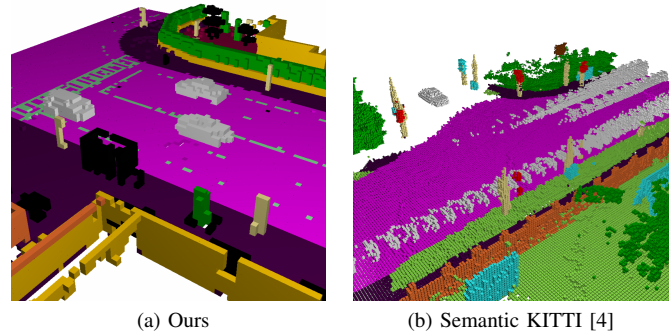


Fig. 1: Side-by-side comparison of our dynamic scene completion data set (left) with Semantic KITTI [4] (right) on dynamic scenes from each respective data set. Moving vehicles, represented in white, leave traces in the KITTI data set yet are accurately and completely represented in our data set. Using multiple viewpoints, we reconstruct a dynamic scene without traces and with minimal occlusions.

Maps provide a unified framework to combine sensor information into a higher level of scene understanding with interpretable information. They store structured information which may be re-purposed later in tasks such as localization and path planning, where algorithms can retrieve locations of landmarks and driveable surfaces. This can provide benefits including increased reliability and predictability in diverse fields such as remote sensing, augmented reality, autonomous vehicles, and even medical devices. Although some research has proposed mapless navigation [5–9], maps are still widely used due to their interpretability and success.

Maps may include multiple layers of information such as traversability, semantic labels, and dynamic occupancy. Traversability maps generally construct a binary go-no-go map which may be used by autonomous vehicles for optimal path planning. Semantic maps include rich semantic labels for each cell, however generally only function in static scenes [10–12]. Dynamic occupancy maps construct binary labels for cells indicating free or occupied, and extend their domain to scenes with dynamic actors by incorporating scene dynamics [13–15]. While learning-based approaches have been attempted in 2D [16, 17], most 3D maps rely on feature engineering which can decrease performance and efficiency.

Although maps are generally hand-crafted algorithms, semantic scene completion (SSC) is a deep learning approach requiring supervision. In SSC, sensor data from a single scan is used to complete a dense local semantic scene where completing the occluded portions of the scene may be accomplished by smoothing. However, the problem constraints leave

time information unused. By adding temporal information, networks could gain insight into occlusions and dynamics and become more similar to supervised 3D semantic mapping algorithms.

The main challenges facing 3D semantic scene understanding are the memory and computation cost of 3D computer vision [3, 18], and the inability to obtain ground truth data in the presence of dynamic objects and occlusion [19–22]. To combat the exponentially increasing cost of 3D computer vision, some approaches include projecting to 2D views such as bird’s-eye-view (BEV) [23–25], spherical-front-view (SFV) [22, 26], point pillars [27], or processing directly in 3D with point operations [28, 29] or sparse convolutions [30, 31]. Some more recent approaches leverage the speed of 2D convolutions while preserving height information by treating the vertical dimension of an occupancy grid as the channel [16, 32]. This method maintains a high inference rate as fast as 100 Hz while achieving high performance in 3D object detection and SSC.

A final challenge facing 3D maps is the availability of data sets. A complete scene is difficult to obtain in the real world due to dynamic objects. While indoor data sets [33–38] may place multiple sensors throughout the scene to construct a 3D environment, this is not feasible for outdoor environments. Furthermore, currently existing synthetic data sets either contain only indoor environments, provide annotations for the scene only visible to the ego sensor, or remove dynamic objects altogether [39]. Therefore, mapping algorithms are commonly evaluated indirectly on object detection or motion prediction tasks. While data sets such as SemanticKITTI [4] offer outdoor semantically labeled scenes, dynamic objects leave traces in the constructed map due to the inconsistency of the scene with respect to time. The lack of a complete outdoor 3D scene makes it impossible to directly learn or evaluate 3D mapping in dynamic, outdoor environments.

In this paper, we propose to learn a real-time network that infers a dense ego-centric 3D semantic map by approaching SSC with temporal information. To quantify performance and supervise learning accurately, we construct a novel synthetic data set containing realistic outdoor driving scenes with complete semantic labels of free and occupied space. By randomly sampling multiple viewpoints of each scene, we ensure minimal occlusions and no traces left by dynamic objects. Our contributions are as follows.

- 1) Develop a real-time deep neural network for 3D semantic mapping in dynamic environments.
- 2) Demonstrate improvement over state-of-the-art semantic scene completion networks quantitatively and qualitatively.
- 3) Create a new complete data set for semantic scene completion and 3D mapping in dynamic outdoor environments to address the shortcomings in existing data sets.
- 4) Open source all data and network software for reproducibility and future developments at <https://github.com/UMich-CURLY/3DMapping>.

II. PRELIMINARIES

We first introduce current scene completion data sets, and modern approaches to the problem of semantic scene completion. We also mention trade-offs in storage methods of scenes, and introduce the motivation behind our choice in baselines.

A. Data sets

Current existing data sets are unable to accurately measure scene completion or mapping performance in outdoor dynamic environments due to occlusions of moving objects. While an indoor scene may be captured from multiple view points simultaneously, this is difficult to do in the real world [40]. Instead, existing data sets sample the ground truth map at time t by aggregating data from sequential frames. However, this produces traces left behind by dynamic actors, which leads to incorrectly labeled free or occupied space. An example of traces and occlusions in a modern scene completion data set is shown in Figure 1b, where dynamic vehicles leave behind long white traces and parts of the scene are completely occluded. Current approaches solve this issue by avoiding dynamic objects altogether through rejection of dynamic objects during map generation or post-rejection of dynamic objects after the map is generated [41]. However, these convoluted methods are due to the inavailability of accurate dynamic scenes, and are not ideal for obtaining a representation of the true, complete scene.

Some of the most popular outdoor scene completion data sets include SemanticKITTI [4] and SemanticPOSS [42], or virtual data sets SynthCity [39] and more recently Paris-CARLA-3D [43]. SemanticKITTI provides densely labeled voxelized scenes, but is susceptible to traces due to aggregating frames temporally, as shown in Figure 1. While aggregating recent data to form a complete frame may aid with completeness, it violates the assumption that the data is independently and identically distributed (i.i.d.), as dynamic objects have moved between frames. SemanticPOSS also provides point clouds and semantic labels in dynamic scenes, yet is still susceptible to occlusions and traces for the same reason. SynthCity solves the issue of traces by removing dynamic objects at the cost of dynamic scenes. Finally, Paris-CARLA-3D provides a mixed synthetic and real data set using a mobile LiDAR sensor, but is still susceptible to traces for the same reason. Without a complete ground truth, it is impossible to correctly quantify performance on outdoor scene completion in dynamic environments, and difficult to supervise learning which properly handles dynamic objects.

When creating a data set for SSC, there are a plethora of scene representations to consider, balancing resolution and information with data compression. Voxel grids are the most popular 3D representation of semantic scenes, however there exist several other less frequently used methods for efficiently storing 3D semantic information [1]. Point clouds are an efficient and direct method for storing scenes, which may be further optimized through meshes. However, both meshes and point clouds remain difficult representations for SSC, and few works have attempted this method due to challenging point generation. Additionally, sampling free space is more

difficult as it is implicitly defined. Structured grids such as voxel grids or occupancy grids have the benefit of directly encoding semantic and free labels, and may be directly processed with convolutions. Despite high memory requirements due to explicitly defining free and occupied regions, their easy usage and interpretability make grids a frequent option. While grids may be implicitly encoded using a gradient field such as Signed Distance Function (SDF) or Truncated Signed Distance Function (TSDF), some SSC networks have found them to require a large computation time and add little benefit [4, 32, 44]. For real-time applications, this trade-off is not practical, and as a result voxel grids are commonly chosen.

B. Semantic Scene Completion

Scene Completion (SC) is a method of inferring the full geometry of a scene using either 2D or 3D observations. While research historically used interpolation methods, a subset of SC known as Semantic Scene Completion (SSC) has become popular due to advances in 3D deep learning networks. SSC differs from traditional SC by jointly inferring both semantics and geometry of the whole scene. Furthermore, the SSC task is made more difficult by the sparsity of the input data and incomplete ground truth, providing weakly guided supervision.

Semantic scene completion is a similar task to semantic mapping, however it is generally defined using sensor data from only a single frame. While there exist some deep learning 3D mapping methods, it is not a common task due to the lack of accurate outdoor dynamic data to supervise and quantify performance on [17, 45–48]. SSC is currently a difficult task with minimal generalizability to real life due to the lack of accurately labeled dynamic scenes, as discussed in the previous section.

There are several approaches to SSC which attempt to balance the complexities of 3D computer vision with a low runtime for practical purposes. 3D computer vision has become a more tractable problem due to innovative approaches such as PointNet [28, 29], PointPillars [27], VoxelNet [18], and sparse convolutions [49, 50]. These networks were able to reduce the memory and computation consumption of directly processing 3D data through viewing the problem in different ways. As a result, scene completion may be formulated in any of these formats through View-Volume networks, Volume networks, Hybrid networks, and Point-based networks [40].

Volume networks consist of 3D convolution to directly accomplish scene completion due to high levels of success in semantic segmentation, and the ability to aggregate contextual information from different levels [51, 52]. This approach is limited by the large memory necessitated by directly processing 3D data, so is generally attempted with sparse convolutions such as in JSC3Net [53]. View-Volume networks such as LMSCNet [32, 54] use 2D convolutions in conjunction with 3D convolutions due to the efficiency of 2D convolutions. One method is to view the vertical axis of the 3D scene as a channel dimension, thus enabling the scene to be processed with 2D convolutions. This approach has also been taken in other 3D deep learning tasks with demonstrable success, such as MotionNet [16] in the task of 3D object detection. A

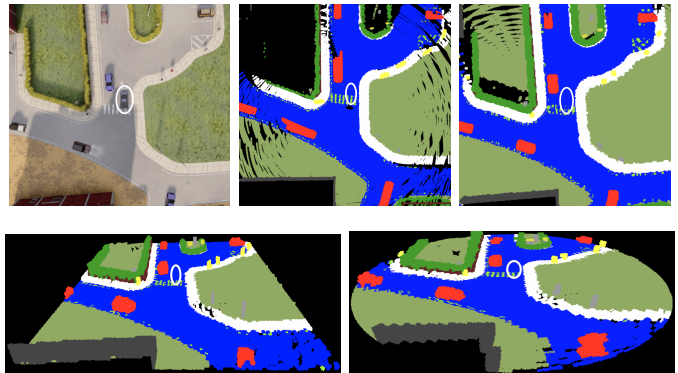


Fig. 2: An illustration of our approach to constructing a 3D dynamic outdoor driving data set. The ego vehicle is circled in all images, and is filtered out of the raw data. Top: The left image shows the Bird’s Eye View (BEV) of a driving frame from Town07 in our data set, the middle image demonstrates the current method of semantic scene generation, and the right image contains our method. Our method is able to accurately label free space and construct more of the scene through the use of additional randomly placed sensors. Bottom: Constructed 3D semantic scene in Cartesian (Left) and Cylindrical (Right) coordinate systems.

segmentation head then lifts the features from 2D to 3D to complete semantic segmentation of the 3D scene. Point-based networks operate directly on points to prevent discretization, but few works have investigated this avenue [55]. Finally, Hybrid networks combine any of the aforementioned methods [4, 44, 56–58].

III. METHOD

Our methodology is split into two sections: first we construct a complete outdoor dynamic data set, and next we train a model from our data set.

A. Data

We create a new outdoor driving semantic scene completion data set with accurate and complete scenes. Our data set is a large synthetic outdoor driving scene completion data set with free space and semantic labels, without the issues of occlusion and traces in Semantic KITTI [4]. We accomplish this by capturing scenes from multiple vantage points using the CARLA [59] simulator. View points are randomized for every driving scene, which supervises networks to generalize to any view. While multiple cameras have been used for indoor static scenes, this is the first synthetic data set to extend the same approach to dynamic scenes. A comparison of our data collection method with currently existing methods is shown in Figure 2. As can be seen, our method obtains a complete semantic scene with minimal occlusions and no traces, in contrast with currently existing dynamic data sets.

We imitate the parameters and structure from the KITTI data set to increase generalizability to real world data, such as the parameters of the on-board LiDAR. Our data set consists of 24 scenes in 8 dynamic maps with road users in various traffic settings. For each frame, we capture the full scene with free space labels by superimposing multiple vantage points of the same scene, and obtaining free space through ray

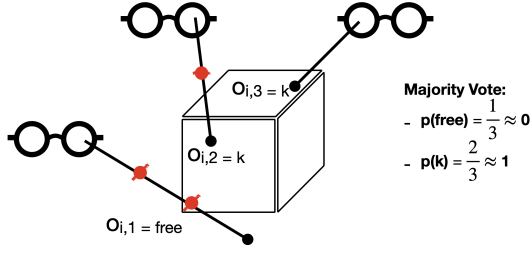


Fig. 3: Toy illustration of how the semantic measurement for a single cell i is obtained. Multiple sensors, shown as eyeglasses, sample points and their semantic labels from the environment. Occupied points are shown in black, and free observations obtained from ray tracing are red. In this case, sensors 2 and 3 observe points in cell i with label k . However, sensor 1 observes a point past the cell, resulting in a free measurement in cell i when ray tracing is computed. Therefore there are two k measurements and one free measurement for cell i , labeled as class k after a majority vote.

tracing. Our data includes point clouds observed by the ego vehicle’s LiDAR sensor with semantic segmentation and ego-compensated scene flow labels, ground truth pose and time labels, and the complete scene. Our data set contains 43,200 frames, which is approximately the same size as KITTI, and may easily be expanded in the future through our open-source software by adding more maps, sensors, or weather conditions.

We generate synthetic data from the CARLA simulator for its high definition, generalizability to the real world, and realism including autonomous pedestrians and vehicles, weather patterns, and traffic. Additionally, the CARLA simulator may be fully synchronized so that we may obtain ground truth pose and sensor data at every frame. While the CARLA API doesn’t provide access to the mesh at each frame, we are able to semantically label the local volume around the ego vehicle by placing multiple sensors around the vehicle.

We create simulated Velodyne 64-E LiDAR sensors, which are the same type used in KITTI [4]. The ego-sensor is placed on board the ego vehicle half a meter backwards from the center of the vehicle, and at the top of the vehicle 1.8 meters above the ground. The sensor samples at a frequency of 10 Hz with 130,000 points per scan created from 64 channels. The maximum range is 50 meters, and points which sample the ego vehicle or an unknown label from the simulator are discarded, creating a clean data set. Uniform noise is added to each point, such that each point is at most 2 centimeters from its true value. Due to the synchronization of the simulator, exact poses for each sensor may be obtained at each step. The pose and time of the ego sensor are recorded in a file for each scene. In addition to raw point clouds, we also record ego-motion compensated scene flow for each point, as well as semantic labels according to the CARLA labeling scheme.

We divide the maps into a train, validation, and test set where the train set contains the first six maps, the validation set contains map Town07, and the test set contains map Town10. Each map is used to create three scenes under low, medium and high traffic conditions. Each scene contains 3 minutes of data sampled at 10 Hz, for a total of 1800 frames.

To create the semantic volume for each frame, we randomly place and attach additional LiDAR surrounding the ego vehicle, then superimpose their scans to obtain a complete

Algorithm 1 Ray Tracing Algorithm

```

1: Require: semantic point cloud  $P_s^t$ , free space step  $r$ 
2:  $O_s^t \leftarrow \emptyset$ 
3: for  $x_i, y_i \in P_s^t$  do
4:    $O_s^t \leftarrow O_s^t \cup (x_i, y_i)$  ▷ Occupied observation
5:    $d \leftarrow \|x_i\| - r$ 
6:    $\hat{x}_i \leftarrow \frac{x_i}{\|x_i\|}$ 
7:   while  $d > 0$  do ▷ Iterate towards sensor
8:      $O_s^t \leftarrow O_s^t \cup (d \cdot \hat{x}_i, \text{free})$  ▷ Free observation
9:      $d \leftarrow d - r$ 
10:  end while
11: end for
12:  $O_s^t \leftarrow T_{0,s} O_s^t$  ▷ Transform to ego-sensor frame
13: Return: sensor observations  $O_s^t$ 

```

scene. By generating point clouds from multiple randomly placed sensors, we obtain voxelized labels more reflective of the true distribution, without the presence of traces and with minimal occlusions. While occlusions are minimized, they are still present, and we randomize LiDAR locations between each scene to counteract this effect. Changing the vantage points of the sensors between each scene ensures that the whole data set is a better representation of the true data distribution, and supervised networks will learn to fill in gaps. By placing the sensors randomly, we assure that our data is i.i.d., which we can show guarantees convergence by the strong law of large numbers as the number of sensors and samples increases.

The number of sensors is constant throughout our data set. At the beginning of each scene, 19 LiDAR sensors (for a total of 20 including the ego sensor) are placed uniformly around the ego vehicle in a rectangular prism 20 meters to either side, and 1 to 5 meters above the vehicle. As previously stated, sensor placement is different for each scene, which supervises network generalizability. Our scenes also contain free space labels, which we obtain by ray tracing from each point to the sensor which obtained the data. Note that our data contains sample of the *visible* world, which includes free space and surfaces of objects.

Let O indicate the set of observations of the visible (not including the interior of objects) world, \mathcal{S} represent the set of randomly placed i.i.d. sensors s , and t be the current time. Then, we can write that:

$$p(O_t) = \int_{\mathcal{S}} p(O_t | s) ds \approx \sum_{i=1}^S p(O_t | s_i). \quad (1)$$

This shows that our sampling method converges to the ground truth and is valid even when there are dynamic objects. This method may be extended to other simulation environments, and possibly to the real world. An example of the raw data produced for a single frame is shown in Figure 2. As can be seen, there are no traces left by dynamic objects, and a more complete view of the scene is available, with fewer occlusions.

$$O^t = \{O_s^t | \forall s \in \mathcal{S}\}. \quad (2)$$

To label free space in our 3D volume, we use ray tracing backwards from each point in the point clouds. Ray tracing is completed by sampling backwards at a constant distance

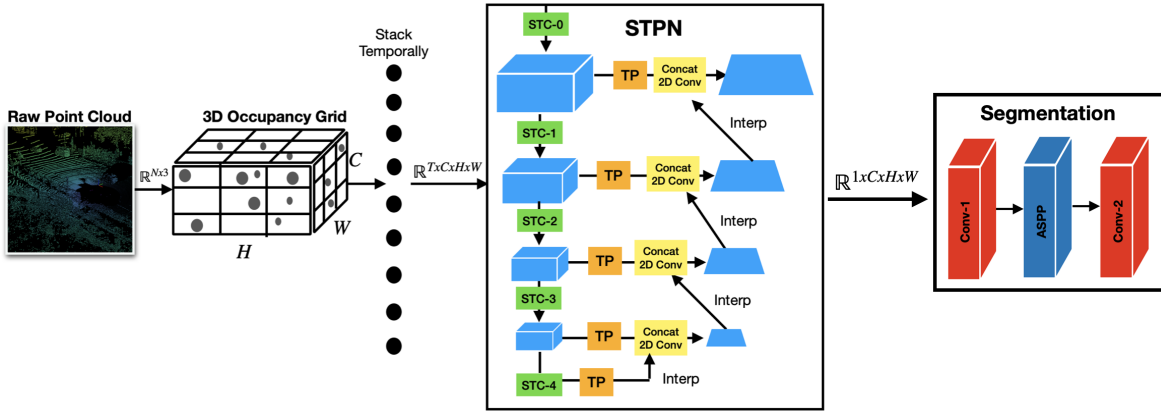


Fig. 4: Proposed MotionSC network. A Spatio-Temporal Pyramid Network [16] backbone performs SSC using temporal information in real-time. The shrinking dimension of the rectangular prism indicates the temporal axis being squeezed from size T to size 1 in the temporal pooling (TP) layer. For specific layer details, please see our website.

of $r = 1.5$ meters until the observing sensor is reached. By sampling in this way, we ensure that free samples are also i.i.d.. An illustration of how cell labels are computed using the multiple sensors and free space sampling is shown in Figure 3. An algorithm for ray tracing is shown in Algorithm 1, where the set of all occupied and free space observations O_s^t for sensor s are computed from the point cloud P_s^t observed by sensor s in its frame of reference. Note that each point contains a geometric position x and a semantic label denoted as y . Once all observations are computed, they are transformed to the on-board ego sensor using a transformation matrix where $s = 0$ represents the ego-matrix. Finally, all observations are combined into one set O^t , which is used to compute the complete semantic scene.

Our data set contains semantically labeled complete scenes in Cartesian and Cylindrical coordinates for each frame, raw ego vehicle LiDAR with semantic and scene flow labels, and ego vehicle poses for each time step. Each semantically labeled scene is of the dimension (128, 128, 8), with roughly equal volumes for Cartesian and Cylindrical coordinate system. Our data contains labels both in front and behind the vehicle, as opposed to Semantic KITTI which voxelizes only the region in front of the ego vehicle. For more information on how to use our data and the specifications, please see our website.

| Remapped Class | Original Classes |
|----------------|---|
| Other | Other, Sky, Bridge, Railtrack, Static, Dynamic, Water |
| Barrier | Fence, Wall, Guardrail |
| Poles | Pole, Traffic Light, Traffic Sign |
| Road | Road, Roadline |
| Ground | Ground, Terrain |

TABLE I: Remapped classes and the original classes they contain.

Our data set includes the raw CARLA labels obtained for every point, however we find that some classes are unobserved or exceedingly difficult to distinguish from one another. Therefore, we also propose a remapping of labels from the initial 23 to a set of 11, shown in Table I.

B. MotionSC: Dense Local Mapping

Next, we create a benchmark neural network on our data set which we compare to the baseline scene completion algorithms. The goal of our method is to create a real-time dense local semantic mapping algorithm which may run on-board mobile robots in outdoor, dynamic scenes. Our network learns to propagate a dynamic scene through time, and learns to convert sequential raw point clouds into a semantically labeled 3D scene including labels for free space. We leverage temporal information and advancements in 3D deep learning to achieve high frequency inference, with the ability to reason about occlusions and dynamic objects. A diagram of our network may be seen in Figure 4.

The input to our network is raw point clouds, which we convert to 3D occupancy grids. We input 3D occupancy grids instead of TSDF format since TSDF format has been found to require a greedy computation time with little benefit [4, 32, 44], which makes it impractical for a real-time dense local mapping algorithm. 3D occupancy grids are created for each frame and maintained in a stack with a maximum depth of T consecutive frames. By leveraging temporal information, we are able to train the network to reason about dynamic objects and occlusions.

The temporal stack of shape $(T \times H \times W \times C)$ is fed to a Spatio-Temporal Pyramid Network (STPN) [16], which treats the vertical axis as a channel dimension C to process the four dimensional grid in real time using 2D convolutions and temporal pooling. In the Euclidean coordinate system, the 3D occupancy grid has dimensions (H, W, C) for the (x, y, z) axes. The STPN is shown in Figure 4, and is a U-Net [61] structure composed of two key components: Temporal Pooling (TP) to aggregate information across frames, and Spatio-Temporal Convolution (STC) to increase feature size while reducing the temporal and spatial (H, W) dimensions. TP is a consistent operation throughout all layers, and applies a 3D max pooling operation to the (C, H, W) dimensions where the *temporal* dimension T is pooled to size 1. STC is a series of 2D convolutions over the (H, W) dimensions to grow the channel size and reduce the spatial dimension by half, sometimes followed by a 3D convolution over the (T, H, W)

| Method | Mean IoU | Accuracy | Free | Building | Barrier | Other | Pedestrian | Pole | Road | Ground | Sidewalk | Vegetation | Vehicles |
|------------------|--------------|--------------|--------------|--------------|-------------|--------------|--------------|--------------|--------------|--------------|--------------|--------------|--------------|
| | | | Free | Building | Barrier | Other | Pedestrian | Pole | Road | Ground | Sidewalk | Vegetation | Vehicles |
| LMSCNet [32] | 39.83 | 94.09 | 97.23 | 27.42 | 2.69 | 10.17 | 24.29 | 43.13 | 87.36 | 16.35 | 45.56 | 32.52 | 51.40 |
| SSCNet [60] | 17.96 | 66.07 | 64.32 | 21.79 | 1.66 | 6.71 | 8.24 | 0.14 | 22.75 | 9.50 | 19.22 | 17.39 | 25.86 |
| SSCNet-Full [60] | 43.17 | 94.46 | 96.03 | 29.94 | 1.65 | 15.29 | 29.76 | 28.57 | 90.94 | 33.04 | 71.38 | 26.42 | 51.85 |
| JS3CNet [53] | 45.01 | 94.68 | 95.83 | 33.40 | 5.41 | 19.30 | 35.22 | 38.05 | 92.30 | 18.83 | 73.29 | 28.09 | 55.36 |
| MotionSC | 42.73 | 94.87 | 97.15 | 28.02 | 1.99 | 7.43 | 34.26 | 37.00 | 90.76 | 25.94 | 60.93 | 33.05 | 53.52 |

TABLE II: Semantic results on test set with reduced classes.

| Method | Mean IoU | Accuracy | Free | Building | Fences | Wall | Guard Rail | Other | Sky | Bridge | Rail Track | Static | Dynamic | Water | Pedestrian | Pole | Traffic Light | Traffic Sign | Road | Road Lines | Ground | Terrain | Sidewalk | Vegetation | Vehicles |
|------------------|--------------|--------------|--------------|--------------|-------------|-------------|------------|-------------|-----|--------|------------|--------------|-------------|-------|--------------|--------------|---------------|--------------|--------------|-------------|-------------|-------------|--------------|--------------|--------------|
| | | | Free | Building | Fences | Wall | Guard Rail | Other | Sky | Bridge | Rail Track | Static | Dynamic | Water | Pedestrian | Pole | Traffic Light | Traffic Sign | Road | Road Lines | Ground | Terrain | Sidewalk | Vegetation | Vehicles |
| LMSCNet [32] | 24.68 | 93.4 | 96.94 | 22.25 | 0.75 | 0.39 | N/A | 0 | N/A | N/A | N/A | 9.63 | 1.31 | N/A | 25.58 | 41.10 | N/A | 3.33 | 82.47 | 0.02 | 1.30 | 2.40 | 46.53 | 36.20 | 49.37 |
| SSCNet [60] | 11.56 | 68.72 | 68.13 | 23.42 | 1.23 | 0.07 | N/A | 0.01 | N/A | N/A | N/A | 6.21 | 3.35 | N/A | 4.85 | 0.51 | N/A | 0 | 20.14 | 0 | 2.62 | 1.29 | 19.04 | 20.46 | 25.20 |
| SSCNet-Full [60] | 25.97 | 93.52 | 95.99 | 29.39 | 1.09 | 0.09 | N/A | 0.15 | N/A | N/A | N/A | 15.15 | 2.92 | N/A | 28.66 | 24.42 | N/A | 6.54 | 84.96 | 0.00 | 5.11 | 3.24 | 69.47 | 25.3 | 49.12 |
| JS3CNet [53] | 30.09 | 94.36 | 96.72 | 29.73 | 1.54 | 0.20 | N/A | 0.12 | N/A | N/A | N/A | 25.97 | 9.85 | N/A | 44.02 | 42.34 | N/A | 0 | 87.34 | 0.02 | 6.52 | 1.73 | 71.40 | 35.81 | 58.23 |
| MotionSC | 26.66 | 94.2 | 97.31 | 26.77 | 0.31 | 0.53 | N/A | 0.01 | N/A | N/A | N/A | 9.09 | 1.85 | N/A | 25.37 | 39.03 | N/A | 11.28 | 83.95 | 0.02 | 1.96 | 3.60 | 61.80 | 37.70 | 52.56 |

TABLE III: Semantic results on test set with all classes.

dimensions with the channel dimension remaining as the features. Upsampling deeper layers to combine with shallow layers is done by interpolation over the (H, W) dimensions a factor of 2, then concatenating with the next sequential layer and applying 2D convolutions. More information on STPN may be found in [16], and our layer hyperparameters may be found on our website. The output of the network is a $(1 \times C \times H \times W)$ dimensional rectangular prism where the temporal dimension has been pooled.

For the segmentation head, we use one of the segmentation heads from [32], which has been shown to be successful raising the dimension of the latent space to include a feature dimension for semantic classes. The goal of the head is to learn semantic classes from the $(1 \times C \times H \times W)$ dimensional cube, and form a $(K \times C \times H \times W)$ dimensional shape encoding the un-normalized probabilities of each class. The segmentation head performs 3D convolutions to lift the feature dimension from 1 to C , learn spatial relations from differently sized residual fields through a sequence of dilations in an Atrous Spatial Pyramid Pooling (ASPP) block [62, 63], and finally lift the feature dimension from C to K , where K is the number of classes. For inference, a softmax layer is applied and the maximum argument along the class K dimension is taken.

IV. RESULTS AND DISCUSSION

We establish several baselines using state-of-the-art open source SSC networks on our data set, then compare our proposed real-time dynamic semantic mapping network, MotionSC, to establish a benchmark. We show that temporal information enhances our network to achieve semantic and geometric completion results on par or better on every metric. We also compare the run-times and model sizes of each network, and show that our network balances performance with efficiency for high-speed applications. Finally, we include a qualitative comparison from images on our test set of each model. Full length videos of the test set are available in the supplementary material.

A. Quantitative Evaluation

We choose to compare our network with LMSCNet [32], SSCNet [60] and JS3CNet [53], as they are the best available

open-source SSC networks at the time. LMSCNet and SSCNet are both high-speed, low memory models designed for efficiency. Following [32], we also include SSCNet-Full, where deconvolution layers are added to SSCNet to account for the downsampled resolution produced by the network. JS3CNet is a sparse 3D convolution network which has a slower inference time making it impractical for real-time applications, but achieves state-of-the-art performance on SSC. While these networks do not take advantage of temporal information, they serve as a strong baseline for MotionSC on our dataset. As mentioned in Section II-B, there are few open-source supervised mapping algorithms for dynamic scenes, and as a result state-of-the-art SSC networks make more competitive baselines. We attempt to imitate the learning parameters and process of each network as closely as possible, and choose the best model according to mean intersection over union (IoU) on the validation set. Models are trained for 24 to 48 hours, and model weights and training data are recorded and are available open source for reference.

All networks are compared over the test set with Euclidean coordinates, both on the full set and reduced set of classes. We compare semantic performance by measuring the accuracy over all semantic classes, and the IoU of each individual class. Classes are color coded to allow for easy interpretation between the full and mapped class sets. Table II shows the results obtained from the reduced set of classes, and Table III shows the results from all classes. The results of the networks are generally mixed when viewed on a per-class basis, as each network performs well on some classes. However, some differences emerge when examining the overall accuracy and mIoU scores. MotionSC performs well on most classes, achieves a higher mIoU and accuracy than the lightweight networks in most cases, and is comparable with the heavier 3D convolution-based JS3CNet. For example, on the set with reduced classes, MotionSC achieves the highest semantic accuracy, and the third highest mIoU.

A similar pattern emerges when measuring performance on geometric completeness, shown in Table IV. Geometric completeness is measured by mapping all non-free semantic classes to a single label, then measuring the precision, recall, and IoU on the binary segmentation task. MotionSC has the

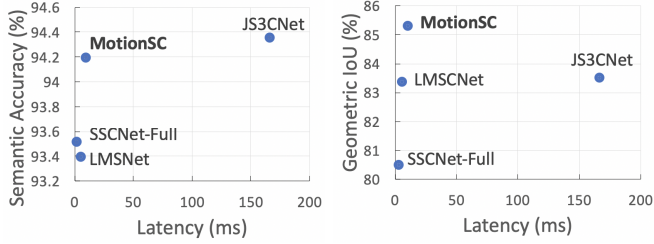


Fig. 5: Scatter plot of average inference time vs. semantic and geometric performance of each method. Inference time was measured on an NVIDIA RTX 3090 GPU by averaging one hundred trials. Semantic accuracy is computed over all classes in the test set, including free space. Geometric performance is also measured on all classes, but is calculated by mapping all non-free semantic classes to a single occupied class. As can be seen, MotionSC predicts an accurate and complete 3D semantic scene while maintaining quick inference times due to its 2D CNN backbone.

| Method | Precision (%) | Recall (%) | IoU (%) |
|----------|---------------|--------------|-------------|
| SSCNet | 30.35 | 66.83 | 26.38 |
| SSC-Full | 86.01 | 92.64 | 80.51 |
| LMSCNet | 95.41 | 86.85 | 83.37 |
| JS3CNet | 89.08 | 93.06 | 83.53 |
| MotionSC | 94.97 | 89.59 | 85.3 |

TABLE IV: Geometric Completeness on full test set. Obtained by mapping all non-zero labels to occupied, and calculating the precision, recall, and intersection over union (IoU) to obtain a measure of completeness.

highest IoU of 85.3%, nearly 2 percent higher than that of JS3CNet. MotionSC also performs well in precision, falling just short of LMSCNet, and on recall, achieving the third highest score. This metric indicates that MotionSC gains some advantage in completeness by leveraging temporal information to mitigate occlusions.

The differences in models are most apparent when comparing the overall semantic accuracy and geometric IoU with model inference time. Figure 5 presents two plots, highlighting the superior performance of MotionSC with its lightweight design. Inference times for each model are obtained by measuring GPU inference time on an NVIDIA GeForce RTX 3090 GPU, averaged over one hundred repetitions. We plot SSCNet-Full instead of SSCNet for a fairer comparison, as it achieves much higher performance on our data set. Although MotionSC has a slightly lower semantic accuracy than JS3CNet on the reduced class set, it operates much faster, similar in speed to SSCNet and LMSCNet. On the geometric completeness plot, MotionSC achieves the best level of completeness due to temporal information, while maintaining a lightweight design. MotionSC achieves a high level of performance on completeness and semantic segmentation of the scene, while maintaining rapid inference.

B. Qualitative Evaluation

We compare each model qualitatively on the test set of our data set. MotionSC achieves a high level of geometric completeness and semantic segmentation due to temporal information. This difference is clear visually, as MotionSC is able to achieve a smoother, more complete scene since it is less susceptible to occlusions and can reason successfully about dynamic objects. We generate predictions for each model on the test sequence, then compare the predictions visually in a side-by-side comparison.

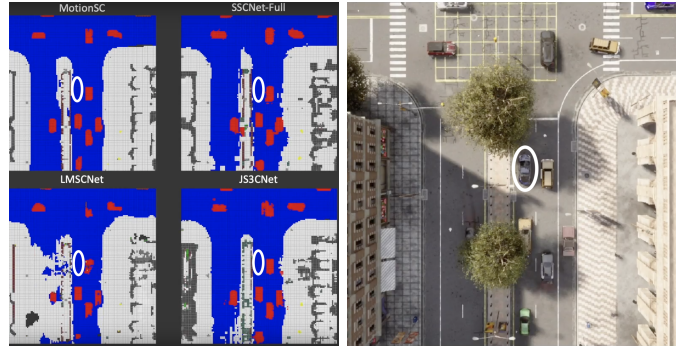


Fig. 6: Qualitative comparison of scene completion networks on a frame from the test set. The left four images show predictions from each network, and the right image shows the ground truth obtained by a camera. All scenes are visualized from a BEV, although the scenes are complete 3D semantic scenes. MotionSC balances a high level of semantic accuracy with geometric completeness due to temporal information, achieving the smoothest prediction. Videos are included on our website.

Figure 6 shows a single frame of a scene from the test set, with predictions by each model, and a ground truth camera image. Each network is able to generate a complete scene with semantic labels to some degree. SSCNet creates a smooth scene, although there is some noise visible in the bottom left corner. It also is unable to complete the left-most car due to an occlusion. LMSCNet is most susceptible to noise due to occlusions, which is evident again in the bottom left corner and in individual vehicles. JS3CNet is also susceptible to noise, but achieves high accuracy and completion at the cost of expensive 3D convolutions. MotionSC in contrast, is able to generate the most smooth scene of the lightweight networks, with the road and sidewalk clearly labeled, and minimum occlusions.

V. CONCLUSION

This paper addressed a need for semantic scene completion data by creating a novel outdoor data set with accurate and complete dynamic scenes. The dataset uses the CARLA simulator [59] with similar parameters to the real-life Semantic KITTI [4] data set to promote generalization in future works. We trained a real-time dense local semantic mapping algorithm to enhance semantic scene completion using temporal information. Our network shows that the proposed data set can quantify and supervise accurate scene completion in the presence of dynamic objects, encouraging future developments of dynamic mapping algorithms by the community.

Future work include improving the MotionSC algorithm to develop a more robust real-time local semantic mapping algorithm by adding recurrency or quantifiable uncertainty. Finally, more work is required to create a real-time mapping network that bridges the gap from simulated to real data.

REFERENCES

- [1] L. Wang and Y. Huang, "A Survey of 3D Point Cloud and Deep Learning-Based Approaches for Scene Understanding in Autonomous Driving," *IEEE Intelligent Transportation Systems Magazine*, 2021.
- [2] J. Janai, F. Güney, A. Behl, and A. Geiger, "Computer vision for autonomous vehicles: Problems, datasets and state of the art," 2021.
- [3] Y. Guo, H. Wang, Q. Hu, H. Liu, L. Liu, and M. Bennamoun, "Deep Learning for 3D Point Clouds: A Survey," *IEEE Trans. Pattern Anal. Mach. Intell.*, vol. 43, no. 12, pp. 4338–4364, 2020.

- [4] J. Behley, M. Garbade, A. Milioto, J. Quenzel, S. Behnke, C. Stachniss, and J. Gall, "A dataset for semantic segmentation of point cloud sequences," *CoRR*, vol. abs/1904.01416, 2019. [Online]. Available: <http://arxiv.org/abs/1904.01416>
- [5] Y. Guo, H. Wang, Q. Hu, H. Liu, L. Liu, and M. Bennamoun, "Deep Learning for 3D Point Clouds: A Survey," *IEEE Trans. Pattern Anal. Mach. Intell.*, vol. 43, no. 12, pp. 4338–4364, 2020.
- [6] M. Bojarski, D. D. Testa, D. Dworakowski, B. Firner, B. Flepp, P. Goyal, L. D. Jackel, M. Monfort, U. Muller, J. Zhang, X. Zhang, J. Zhao, and K. Zieba, "End to end learning for self-driving cars," *CoRR*, vol. abs/1604.07316, 2016. [Online]. Available: <http://arxiv.org/abs/1604.07316>
- [7] F. Codevilla, M. Müller, A. Dosovitskiy, A. M. López, and V. Koltun, "End-to-end driving via conditional imitation learning," *CoRR*, vol. abs/1710.02410, 2017. [Online]. Available: <http://arxiv.org/abs/1710.02410>
- [8] H. L. Chiang, A. Faust, M. Fiser, and A. G. Francis, "Learning navigation behaviors end to end," *CoRR*, vol. abs/1809.10124, 2018. [Online]. Available: <http://arxiv.org/abs/1809.10124>
- [9] L. Tai, G. Paolo, and M. Liu, "Virtual-to-real deep reinforcement learning: Continuous control of mobile robots for mapless navigation," *CoRR*, vol. abs/1703.00420, 2017. [Online]. Available: <http://arxiv.org/abs/1703.00420>
- [10] L. Gan, R. Zhang, J. W. Grizzle, R. M. Eustice, and M. Ghaffari, "Bayesian Spatial Kernel Smoothing for Scalable Dense Semantic Mapping," *IEEE Robotics and Automation Letters*, vol. 5, no. 2, pp. 790–797, 2020.
- [11] L. Sun, Z. Yan, A. Zaganidis, C. Zhao, and T. Duckett, "Recurrent-OctoMap: Learning State-Based Map Refinement for Long-Term Semantic Mapping with 3-D-Lidar Data," *IEEE Robotics and Automation Letters*, vol. 3, no. 4, pp. 3749–3756, 2018.
- [12] C. Zhao, L. Sun, P. Purkait, T. Duckett, and R. Stolkin, "Dense RGB-D semantic mapping with pixel-voxel neural network," *Sensors*, vol. 18, no. 9, 2018.
- [13] Y. Min, D.-u. Kim, and H.-I. Choi, "Kernel-Based 3-D Dynamic Occupancy Mapping with Particle Tracking," no. Icara, pp. 5268–5274, 2021.
- [14] A. Unnikrishnan, J. Wilson, L. Gan, A. Capodiceci, P. Jayakumar, K. Barton, and M. Ghaffari, "Dynamic Semantic Occupancy Mapping using 3D Scene Flow and Closed-Form Bayesian Inference," pp. 1–9, 2021. [Online]. Available: <http://arxiv.org/abs/2108.03180>
- [15] D. Nuss, S. Reuter, M. Thom, T. Yuan, G. Krehl, M. Maile, A. Gern, and K. Dietmayer, "A random finite set approach for dynamic occupancy grid maps with real-time application," *Int. J. Robot. Res.*, vol. 37, no. 8, pp. 841–866, 2018.
- [16] P. Wu, S. Chen, and D. N. Metaxas, "MotionNet: Joint Perception and Motion Prediction for Autonomous Driving Based on Bird's Eye View Maps," *Proc. IEEE Conf. Comput. Vis. Pattern Recog.*, pp. 11 382–11 392, 2020.
- [17] E. Amirloo, M. Rohani, E. Banijamali, J. Luo, and P. Poupart, "Self-Supervised Simultaneous Multi-Step Prediction of Road Dynamics and Cost Map," 2021. [Online]. Available: <http://arxiv.org/abs/2103.01039>
- [18] Y. Zhou and O. Tuzel, "Voxelnet: End-to-end learning for point cloud based 3d object detection," 2017.
- [19] L. Xiao, J. Wang, X. Qiu, Z. Rong, and X. Zou, "Dynamic-SLAM: Semantic monocular visual localization and mapping based on deep learning in dynamic environment," *Robot. and Auton. Syst.*, vol. 117, pp. 1–16, 2019.
- [20] D. Kondermann, R. Nair, K. Honauer, K. Krispin, J. Andrusis, A. Brock, B. Gusefeld, M. Rahimimoghaddam, S. Hofmann, C. Brenner, and B. Jahne, "The hci benchmark suite: Stereo and flow ground truth with uncertainties for urban autonomous driving," in *CVPR Workshops*, June 2016.
- [21] S. R. Richter, V. Vineet, S. Roth, and V. Koltun, "Playing for data: Ground truth from computer games," in *Proc. European Conf. Comput. Vis.*, B. Leibe, J. Matas, N. Sebe, and M. Welling, Eds. Cham: Springer International Publishing, 2016, pp. 102–118.
- [22] B. Wu, A. Wan, X. Yue, and K. Keutzer, "Squeezeseg: Convolutional neural nets with recurrent crf for real-time road-object segmentation from 3d lidar point cloud," 2017.
- [23] F. J. Lawin, M. Danelljan, P. Tosteberg, G. Bhat, F. S. Khan, and M. Felsberg, "Deep projective 3d semantic segmentation," 2017.
- [24] A. Boulch, B. Le Saux, and N. Audebert, "Unstructured point cloud semantic labeling using deep segmentation networks," *3DOR@ Eurographics*, vol. 3, 2017.
- [25] X. Chen, H. Ma, J. Wan, B. Li, and T. Xia, "Multi-view 3d object detection network for autonomous driving," 2017.
- [26] A. Milioto, I. Vizzo, J. Behley, and C. Stachniss, "RangeNet++: Fast and Accurate LiDAR Semantic Segmentation," in *Proc. IEEE/RSS Int. Conf. Intell. Robots and Syst.*, 2019.
- [27] A. H. Lang, S. Vora, H. Caesar, L. Zhou, J. Yang, and O. Beijbom, "Pointpillars: Fast encoders for object detection from point clouds," *Proc. IEEE Conf. Comput. Vis. Pattern Recog.*, vol. 2019-June, pp. 12 689–12 697, 2019.
- [28] C. R. Qi, H. Su, K. Mo, and L. J. Guibas, "Pointnet: Deep learning on point sets for 3d classification and segmentation," *CoRR*, vol. abs/1612.00593, 2016. [Online]. Available: <http://arxiv.org/abs/1612.00593>
- [29] C. R. Qi, L. Yi, H. Su, and L. J. Guibas, "PointNet++: Deep hierarchical feature learning on point sets in a metric space," *Proc. Advances Neural Inform. Process. Syst. Conf.*, vol. 2017-December, pp. 5100–5109, 2017.
- [30] Y. Yan, Y. Mao, and B. Li, "Second: Sparsely embedded convolutional detection," *Sensors*, vol. 18, no. 10, p. 3337, 2018.
- [31] C. Choy, J. Gwak, and S. Savarese, "4d spatio-temporal convnets: Minkowski convolutional neural networks," 2019.
- [32] L. Roldao, R. De Charette, and A. Verroust-Blondet, "LMSCNet: Lightweight Multiscale 3D Semantic Completion," *Proceedings - 2020 International Conference on 3D Vision, 3DV 2020*, pp. 111–119, 2020.
- [33] P. K. Nathan Silberman, Derek Hoiem and R. Fergus, "Indoor segmentation and support inference from rgb-d images," in *Proc. European Conf. Comput. Vis.*, 2012.
- [34] A. Chang, A. Dai, T. Funkhouser, M. Halber, M. Nießner, M. Savva, S. Song, A. Zeng, and Y. Zhang, "Matterport3d: Learning from rgb-d data in indoor environments," 2017.
- [35] B.-S. Hua, Q.-H. Pham, D. T. Nguyen, M.-K. Tran, L.-F. Yu, and S.-K. Yeung, "Scenenn: A scene meshes dataset with annotations," *International Conference on 3D Vision (3DV)*, pp. 92–101, 2016.
- [36] A. Dai, A. X. Chang, M. Savva, M. Halber, T. Funkhouser, and M. Nießner, "ScanNet: Richly-annotated 3d reconstructions of indoor scenes," 2017.
- [37] J. Xiao, A. Owens, and A. Torralba, "Sun3d: A database of big spaces reconstructed using sfm and object labels," in *Proc. IEEE Int. Conf. Comput. Vis.*, 2013, pp. 1625–1632.
- [38] S. Song, F. Yu, A. Zeng, A. X. Chang, M. Savva, and T. Funkhouser, "Semantic scene completion from a single depth image," *Proc. IEEE Conf. Comput. Vis. Pattern Recog.*, 2017.
- [39] D. Griffiths and J. Boehm, "SynthCity: A large scale synthetic point cloud," pp. 1–6, 2019. [Online]. Available: <http://arxiv.org/abs/1907.04758>
- [40] L. Roldao, R. de Charette, and A. Verroust-Blondet, "3d semantic scene completion: a survey," *CoRR*, vol. abs/2103.07466, 2021. [Online]. Available: <https://arxiv.org/abs/2103.07466>
- [41] H. Lim, S. Hwang, and H. Myung, "ERASOR: Egocentric Ratio of Pseudo Occupancy-Based Dynamic Object Removal for Static 3D Point Cloud Map Building," *IEEE Robotics and Automation Letters*, vol. 6, no. 2, pp. 2272–2279, 2021.
- [42] Y. Pan, B. Gao, J. Mei, S. Geng, C. Li, and H. Zhao, "Semanticpos: A point cloud dataset with large quantity of dynamic instances," *CoRR*, vol. abs/2002.09147, 2020. [Online]. Available: <https://arxiv.org/abs/2002.09147>
- [43] J. E. Deschaud, D. Duque, J. P. Richa, S. Velasco-Forero, B. Marcotegui, and F. Goulette, "Paris-carla-3D: A real and synthetic outdoor point cloud dataset for challenging tasks in 3D mapping," *Remote Sensing*, vol. 13, no. 22, pp. 1–24, 2021.
- [44] M. Garbade, Y. T. Chen, J. Sawatzky, and J. Gall, "Two stream 3D semantic scene completion," *Proc. IEEE Conf. Comput. Vis. Pattern Recog.*, vol. 2019-June, pp. 416–425, 2019.
- [45] Y. Xiang and D. Fox, "DA-RNN: Semantic mapping with Data Associated Recurrent Neural Networks," *Robotics: Science and Systems*, vol. 13, 2017.
- [46] S. Lionar, L. Schmid, C. Cadena, R. Siegwart, and A. Cramariuc, "NeuralBlox: Real-Time Neural Representation Fusion for Robust Volumetric Mapping," [Online]. Available: <https://github.com/ethz-asl/neuralblox>
- [47] L. Sun, Z. Yan, A. Zaganidis, C. Zhao, and T. Duckett, "Recurrent-OctoMap: Learning State-Based Map Refinement for Long-Term Semantic Mapping with 3-D-Lidar Data," *IEEE Robotics and Automation Letters*, vol. 3, no. 4, pp. 3749–3756, 2018.
- [48] C. Zhao, L. Sun, P. Purkait, T. Duckett, and R. Stolkin, "Dense RGB-D semantic mapping with pixel-voxel neural network," *Sensors*, vol. 18, no. 9, 2018.
- [49] C. Choy, J. Gwak, and S. Savarese, "4D spatio-temporal convnets: Minkowski convolutional neural networks," *Proc. IEEE Conf. Comput. Vis. Pattern Recog.*, vol. 2019-June, pp. 3070–3079, 2019.
- [50] B. Graham, M. Engelcke, and L. van der Maaten, "3d semantic segmentation with submanifold sparse convolutional networks," *Proc. IEEE Conf. Comput. Vis. Pattern Recog.*, 2018.
- [51] X. Yan, J. Gao, J. Li, R. Zhang, Z. Li, R. Huang, and S. Cui, "Sparse Single Sweep LiDAR Point Cloud Segmentation via Learning Contextual Shape Priors from Scene Completion," 2020. [Online]. Available: <http://arxiv.org/abs/2012.03762>
- [52] J. Zhang, H. Zhao, A. Yao, Y. Chen, L. Zhang, and H. Liao, "Efficient semantic scene completion network with spatial group convolution," *Lecture Notes in Computer Science*, vol. 11216 LNCS, pp. 749–765, 2018.
- [53] X. Yan, J. Gao, J. Li, R. Zhang, Z. Li, R. Huang, and S. Cui, "Sparse Single Sweep LiDAR Point Cloud Segmentation via Learning Contextual Shape Priors from Scene Completion," 2020. [Online]. Available: <http://arxiv.org/abs/2012.03762>
- [54] Y. Guo and X. Tong, "View-volume network for semantic scene completion from a single depth image," *IJCAI International Joint Conference on Artificial Intelligence*, vol. 2018-July, pp. 726–732, 2018.
- [55] M. Zhong and G. Zeng, "Semantic point completion network for 3D semantic scene completion," *Frontiers in Artificial Intelligence and Applications*, vol. 325, pp. 2824–2831, 2020.
- [56] Y. Cai, X. Chen, C. Zhang, K.-Y. Lin, X. Wang, and H. Li, "Semantic Scene Completion via Integrating Instances and Scene in-the-Loop," pp. 324–333, 2021.
- [57] R. Cheng, C. Agia, Y. Ren, X. Li, and L. Bingbing, "S3CNet: A Sparse Semantic Scene Completion Network for LiDAR Point Clouds," no. CoRL, 2020. [Online]. Available: <http://arxiv.org/abs/2012.09242>
- [58] C. B. Rist, D. Emmerichs, M. Enzweiler, and D. M. Gavrila, "Semantic Scene Completion using Local Deep Implicit Functions on LiDAR Data," pp. 1–19, 2020. [Online]. Available: <http://arxiv.org/abs/2011.09141>
- [59] A. Dosovitskiy, G. Ros, F. Codevilla, A. Lopez, and V. Koltun, "CARLA: An open urban driving simulator," in *Proceedings of the 1st Annual Conference on Robot Learning*, 2017, pp. 1–16.
- [60] S. Song, F. Yu, A. Zeng, A. X. Chang, M. Savva, and T. Funkhouser, "Semantic scene completion from a single depth image," *Proc. IEEE Conf. Comput. Vis. Pattern Recog.*, vol. 2017-Janua, pp. 190–198, 2017.
- [61] O. Ronneberger, P. Fischer, and T. Brox, "U-net: Convolutional networks for biomedical image segmentation," 2015.
- [62] L. Chen, G. Papandreou, I. Kokkinos, K. Murphy, and A. L. Yuille, "DeepLab: Semantic image segmentation with deep convolutional nets, atrous convolution, and fully connected crfs," *CoRR*, vol. abs/1606.00915, 2016. [Online]. Available: <http://arxiv.org/abs/1606.00915>
- [63] S. Liu, Y. HU, Y. Zeng, Q. Tang, B. Jin, Y. Han, and X. Li, "See and think: Disentangling semantic scene completion," in *Proc. Advances Neural Inform. Process. Syst. Conf.*, vol. 31. Curran Associates, Inc., 2018.